# Fluid absorption and active and passive ion flows in the rabbit superficial pars recta

JAMES A. SCHAFER, CLIFFORD S. PATLAK, AND THOMAS E. ANDREOLI
*Division of Nephrology, Department of Medicine, and Department of Physiology and Biophysics, University of Alabama in Birmingham, Birmingham, Alabama 35294; and Theoretical Statistics and Mathematics Branch, National Institute of Mental Health, Bethesda, Maryland 20014*

SCHAFER, JAMES A., CLIFFORD S. PATLAK, AND THOMAS E. ANDREOLI. *Fluid absorption and active and passive ion flows in the rabbit superficial pars recta.* Am. J. Physiol. 233(2): F154–F167, 1977 or Am. J. Physiol.: Renal Fluid Electrolyte Physiol. 2(2): F154–F167, 1977.—Isolated rabbit proximal straight tubules were perfused with Krebs-Ringer buffers containing 127.8 mM NaCl and 3.8 mM $NaHCO_3$ (pH 6.6), and bathed with Krebs-Ringer buffers containing 105 mM NaCl and 25 mM $NaHCO_3$ (pH 7.4). Na isethionate replaced Na acetate in both mediums; acetate omission had no effect on net volume absorption ($J_v$, nl $min^{-1}$ $mm^{-1}$). In acetate-free mediums, $J_v$ was 0.41 ± 0.04 (SE) at 37°C and 0.16 ± 0.01 at 21°C. $J_v$ at 21°C was referable to passive driving forces. The transepithelial voltage was +2.7 mV (lumen positive) at 37°C and rose to +3.7 mV at 21°C. At 37°C, net $Cl^-$ absorption accounted for 85 ± 3% of net cation absorption. The data were analyzed in terms of model calculations with flow-diffusion equations for lateral intercellular spaces. Approximately one-third of the $Na^+$ absorption at 37°C could be accounted for by dissipative transport processes; the remainder was active. The computed ionic concentrations along the entire length of intercellular spaces were nearly identical to the ionic concentrations in the bathing solutions, and passive ion transport across the epithelium was accurately predicted from bulk phase ion concentrations. With intercellular spaces isosmotic to the external solutions, fluid absorption could be accounted for in terms of the oppositely directed gradients of $Cl^-$ and $HCO_3^-$ across junctional complexes, because the junctional complexes were more permeable to $Cl^-$ than $HCO_3^-$.

proximal straight tubule; net volume absorption; sodium transport; chloride transport; bicarbonate transport; mathematical model

THE PURPOSE OF THIS PAPER is to present a model which assesses active and passive ion transport and coupled fluid transport in superficial rabbit proximal straight tubules exposed to asymmetrical solutions. In 1962 Curran and MacIntosh (7) showed that osmotic volume flow could occur between two isosmotic external solutions separated by two membranes enclosing a stirred central compartment. Volume flow between the two external solutions depended on the two membranes having varying reflection coefficients, and on the generation of hydrostatic pressure gradients within the central compartment. These workers argued that a comparable series membrane arrangement might account for isotonic fluid absorption coupled to active solute transport in epithelia if active solute transport generated the equivalent of central compartment hypertonicity. Patlak et al. (24) developed a quantitative description of solute and solvent flows across composite membrane systems.

Diamond and Bossert (9) proposed a unique modification of this model to rationalize isotonic fluid absorption across epithelia exposed to symmetrical solutions. They reasoned that active salt transport from apical (luminal) solutions into unstirred intercellular spaces might raise the osmolality of the latter, thereby providing a driving force for osmotic volume flow from cells to intercellular spaces. By assigning active transport sites to the apical ends of intercellular spaces, and assuming a relatively high value for the diffusion resistance of intercellular spaces, Diamond and Bossert (9) computed that during isotonic fluid absorption in actively transporting epithelia intercellular spaces might contain a standing osmotic gradient, progressing from hypertonicity at the closed ends of intercellular spaces to isotonicity at the open ends.

Recent observations from this laboratory (31) indicate that under certain circumstances a standing gradient mechanism may not account for fluid absorption in isolated mammalian superficial proximal straight tubules. When these tubules were exposed to asymmetrical, 300 mosmol $liter^{-1}$ Krebs-Ringer (KR) buffers (the perfusate was a Cl-KR solution with 138.6 mM $Cl^-$, 10 mM acetate, and 3.8 mM $HCO_3^-$ at pH 6.6, and the bath was an $HCO_3$-KR bath containing 113.6 mM $Cl^-$, 10 mM acetate, and 25 mM $HCO_3^-$ at pH 7.4), and active $Na^+$ transport was inhibited, NaCl was absorbed passively and isotonic fluid absorption was coupled to this dissipative salt flux.

We solved the flow-diffusion equations for lateral intercellular spaces of these tubules in terms of measured transepithelial ionic permeability coefficients, the measured rate of dissipative salt absorption, the measured rate of coupled fluid transport, and a variable dimensionless parameter termed $\alpha$, which expressed the ratio of the ionic diffusion resistance of the epithelium with respect to that of an equivalent thickness of free Krebs-Ringer buffer (31). Our calculations indicated that for values of $\alpha$ based on the measured transepithelial electrical resistance of these tubules (20), the $Na^+$, $Cl^-$, and

$HCO_3^-$ concentration in intercellular spaces were uniform as a function of channel length, and very nearly in equilibrium with the bathing solutions. Because the intercellular spaces were isosmotic with external solutions, fluid absorption linked to passive ion absorption could be rationalized entirely in terms of an extracellular rather than a transcellular route. The driving force for fluid absorption could be accounted for quantitatively by the osmotic pressure gradient referable to the oppositely directed $Cl^-$ and $HCO_3^-$ concentration gradients across junctional complexes, and the fact that the latter were more permeable to $Cl^-$ than to $HCO_3^-$ (31).

It is clearly relevant to evaluate salt and water absorption from these tubules under circumstances in which both active and passive ion transport processes are occurring with particular regard to two issues: the relative contributions of active and passive transport processes to net $Na^+$ absorption when these tubules are exposed to asymmetrical Krebs-Ringer solutions resembling those which might be seen by the superficial pars recta in vivo, and the nature of the driving force for fluid absorption under such conditions. In this context, our earlier experimental data (31) on fluid absorption at 37°C from superficial proximal straight tubules exposed to asymmetrical solutions involve a measure of complexity not currently amenable to such an analysis. The experiments were carried out with acetate-containing solutions, and recent observations from this laboratory (29) have indicated that in these tubules acetate is actively absorbed from luminal fluids by as yet undetermined processes, e.g., active transport and/or metabolic consumption.

Therefore, in this paper we extend the analytical model developed previously (31) to experimental data on fluid absorption from proximal straight tubules exposed at 37°C to acetate-free asymmetrical solutions, specifically, a pH 6.6 Cl-KR* buffer in the perfusate, and a pH 7.4 $HCO_3$-KR* buffer in the bath (the asterisk denotes an acetate-free solution). The experimental results indicate that omission of acetate from both perfusing and bathing mediums had no significant effect on the rate of net fluid absorption, either at 37° or at 21°C; and in acetate-free mediums at 37°C, $Cl^-$ was the counter-ion for approximately 85% of $Na^+$ in an isotonic fluid absorbate. The calculations based on the analytical model are consistent with the view that in asymmetrical acetate-free solutions at 37°C, approximately one-third of $Na^+$ absorption from these tubules depended on dissipative transport processes, and the remainder on active $Na^+$ transport. Net fluid absorption may have occurred via an extracellular route when intercellular spaces were isosmotic to external solutions, driven by an osmotic pressure gradient referable to oppositely directed concentration gradients for NaCl and $NaHCO_3$ across junctional complexes. A preliminary report of some of the observations in this paper has appeared elsewhere (32).

## METHODS

The techniques used for studying transport events in proximal straight tubules isolated from superficial regions of rabbit renal cortex are similar to those developed originally by Burg et al. (4) and Kokko et al. (18). Details of the methodology utilized in this laboratory have been presented previously (29, 31, 33); unless otherwise indicated, these techniques were utilized without modification in the present experiments.

Stated briefly, 2.5- to 4.0-mm segments of proximal straight tubules were obtained by gentle teasing from cortical and outer medullary regions of rabbit renal cortex. The dissections were carried out at 0–5°C in the $HCO_3$-KR bathing mediums described below. The isolated tubule segments were transferred to a thermoregulated (±0.5°C) chamber, sucked into holding and collecting pipettes, and perfused with a microsyringe pump in series with a perfusion pipette which was advanced approximately 0.2 mm into the tubule lumen.

The experiments reported in this paper will be analyzed in part by utilizing transepithelial ionic permeability coefficients ($P_{D_i}$, cm $s^{-1}$), determined in many instances from unidirectional tracer fluxes, and the transepithelial water permeability ($P_f$, cm $s^{-1}$), determined from net volume fluxes in the presence of hydrostatic pressure gradients. It is particularly relevant, therefore, to comment on the possibility of bulk phase unstirred layer effects in the isolated tubule preparation, particularly since recent observations from this (30) and other laboratories (40) indicate clearly that bulk phase unstirred layers may result in significant errors, not only in assessing $P_{D_i}$ at zero volume flow, but also in measuring water permeability coefficients from steady-state net volume flows.

As indicated previously (28, 31), when the bathing solutions in the isolated tubule preparation are bubbled with gas, oscillatory motion of the tubules occurs at a rate of 60–200 $min^{-1}$, and convective mixing of minute particles in the bath is evident as near as $2 \times 10^{-4}$ cm to the tubules. Under these conditions, tracer permeability coefficients having values of approximately $15 \times 10^{-4}$ cm $s^{-1}$ [i.e., at least 10-fold greater than either $P_{Na}$ or $P_{Cl}$ (31, 33)] are unaffected by 10-fold increments in the viscosities of both the perfusate and the bath (28). It seems improbable, therefore, that bulk phase unstirred layer effects were a significant factor in the present experiments.

The constituents of the various Krebs-Ringer perfusing and bathing solutions are listed in Table 1. The acetate-containing $HCO_3$–KR and Cl–KR solutions were those described previously (31, 33); the acetate-free counterparts of these solutions were identical except that acetate was replaced by isethionate, a poorly permeant, nonactively transported species (29, 31). As indicated in Table 1, the acetate-free KR solutions have been denoted by asterisks.

The perfusate/bath $Cl^-$ concentration ratio (Table 1; perfusate/bath $Cl^-$ concentration ratio = 1.22) and transepithelial pH gradient were chosen to resemble the values which might be seen in vivo by this nephron segment. To our knowledge, tubular fluid/plasma $Cl^-$ ratios for the pars recta of mammalian species are not available from in vivo micropuncture data; nor are there data providing $Cl^-$ tubular fluid/plasma ratios for in vivo late proximal convolutions in the rabbit. In the rat, the tubular fluid/plasma $Cl^-$ concentration ratios ob-

TABLE 1. *Composition of solutions*

| | Perfusate | | Bath | |
|---|---|---|---|---|
| | Cl-KR | Cl-KR* | $HCO_3$-KR | $HCO_3$-KR* |
| | mM | | mM | |
| NaCl | 127.8 | 127.8 | 105 | 105 |
| $NaHCO_3$ | 3.8 | 3.8 | 25 | 25 |
| Na isethionate | 0 | 10 | 0 | 10 |
| Na acetate. | 10 | 0 | 10 | 0 |
| $Na_2HPO_4/NaH_2PO_4$ | 4 | 4 | 4 | 4 |
| KCl | 5 | 5 | 5 | 5 |
| $CaCl_2$ | 1.8 | 1.8 | 1.8 | 1.8 |
| $MgSO_4$ | 1 | 1 | 1 | 1 |
| Glucose | 0 | 0 | 8.3 | 8.3 |
| L-alanine | 0 | 0 | 5 | 5 |
| Urea | 13.3 | 13.3 | 0 | 0 |
| Albumin | 0 | 0 | 6% | 6% |
| pH | 6.6 | 6.6 | 7.4 | 7.4 |

The various KR solutions were bubbled continuously with 95% $O_2$-5% $CO_2$ and adjusted to the indicated pH. All solutions were adjusted to 300 mosmol liter$^{-1}$. The acetate-free solutions are denoted by an asterisk.

tained from micropuncture of late proximal convolutions are in the range 1.20–1.30 (11, 22, 38); and fluid from late proximal convolutions has a pH in the range 6.7–7.0 (11, 22, 36). Comparable values of pH and $Cl^-$ concentrations have been reported for fluid from late proximal convolutions in other mammalian species, including the dog (6) and monkey (2). Since further acidification of tubular fluid in mammalian species occurs between late proximal convolutions and early distal tubules (11, 12, 36), the compositions of the Cl-KR and Cl-KR* perfusates in Table 1 appear reasonable.

Net fluid absorption ($J_v$, nl min$^{-1}$ mm$^{-1}$ of tubule length) was measured as described previously (29, 31, 33) from the difference between perfusion and collection rates, using exhaustively dialyzed [methoxy-$^3$H]inulin as the volume marker; a positive sign for $J_v$ denotes volume efflux from lumen to bath. The mean internal diameter of these tubules is $22.3 \times 10^{-4}$ cm (33); thus $J_v$ values may be converted from nl min$^{-1}$ mm$^{-1}$ to cm$^3$ s$^{-1}$ cm$^{-2}$ by the factor $2.38 \times 10^{-5}$ cm min mm nl$^{-1}$ s$^{-1}$ (33). The radioactive volume marker was also used to detect leakage into bathing solutions; in the experiments reported, the leakage rate into the bath was uniformly $\leq$1% of the perfusion rate.

The $J_v$ measurements in the present experiments were in the range 0.1–0.45 nl min$^{-1}$ mm$^{-1}$ for tubules 2.5–4.0 mm in length; for isolated proximal convoluted tubules, $J_v$ values in the range of 1.0 nl min$^{-1}$ mm$^{-1}$ have been reported for segments 0.5–1.5 mm in length (13, 18). In other words, although $J_v$ is smaller for straight tubules than for proximal convolutions, absolute differences between perfusion and collection rates, and, hence, the precision of $J_v$ measurements are comparable in the two segments.

Because many of the fluid absorption rates given in this paper were in the range of 0.1–0.2 nl min$^{-1}$ mm$^{-1}$, we have computed the extent to which random variations in radioactivity counting might account for such $J_v$ values. In the experiments reported in this paper (32 tubules), the mean tubule length was 3.25 ± 0.08 mm (mean ± SE), the mean perfusion rate was 10.77 ± 0.45 nl min$^{-1}$, and the mean [$^3$H]inulin radioactivity in the perfusing solutions was 30.64 ± 1.58 counts/min nl$^{-1}$. The collected fluid was sampled at 7–10 min intervals, and in all cases perfusing solution standards and collected fluid samples were counted for 10-min periods. With the same perfusing solutions, the coefficient of variation for the liquid scintillation counter used in our laboratory is, at a maximum, ± 0.3% for a 10-min counting period.

Accordingly, in an average 3.25-mm length tubule perfused for 8 min at 10.77 nl min$^{-1}$ with a solution containing 30.64 counts/min nl$^{-1}$ [$^3$H]inulin, the total radioactivity collected (in the absence of bath leaks) was 26,399 counts per 10 min with an average random variation of ± 80 counts per 10 min. Thus the random error in estimating perfusion rate would be ± 0.033 nl min$^{-1}$, which, for a tubule length of 3.25 mm, could result in errors in $J_v$ measurements amounting to approximately 0.01 nl min$^{-1}$ mm$^{-1}$, or about 10% of the lowest observed $J_v$ value which was significantly different from zero.

Transepithelial voltages ($V_e$, mV, lumen with respect to bath) were measured as described previously (29, 31, 33) with glass 0.9% NaCl/4% agar electrodes placed in both perfusing and bathing solutions. The electrodes were connected via Tygon tubing filled with 3 M KCl to calomel half-cells. Observed voltages were corrected for liquid junction potentials with a form of the Henderson equation (21) modified in terms of ionic activities (1). The mobility of isethionate was obtained from Caldwell (5). As reported previously (31), the liquid junction potential corrections for asymmetrical solutions, e.g., a Cl-KR* perfusate and an $HCO_3$-KR* bath, amounted to 40–60% of the observed $V_e$. Since the length constant for the pars recta is approximately $10^{-2}$ cm (20), $V_e$ measurements in the present paper provide direct information only about electrical events within, at best, 0.02 cm from the inner perfusion pipette.

The chloride concentrations in perfusing and collected fluids were measured as described previously (29) with a microtitration method (25). In experiments in which the $Cl^-$ concentration of collected fluid was determined, samples for $J_v$ measurements were alternated with samples for $Cl^-$ measurements. The latter were stored in glass micropipettes between oil columns until the day after the experiment. All samples of collected fluid were compared to standard solutions having varying NaCl concentrations but the same concentrations of all the other constituents as the perfusing solutions. For the sake of uniformity, samples of perfusing solutions were treated in the same manner and also analyzed for $Cl^-$ concentrations with the ultramicro method. Duplicate ultramicro and large-sample determinations (with an Amico-Cotlove chloride titrator, American Instrument Co., Silver Springs, Md.) of chloride concentrations agreed within 2%.

Computer programs were written in Basic Language and were run on a remote terminal of an IBM model 370-155 computer system at the Division of Biophysical Sciences, University of Alabama in Birmingham, Birmingham, Ala. Reagents, isotope counting techniques, and chemical determinations were as described previously (29, 31, 33).

Measurements in a given tubule were used to compute a mean value for that tubule. Generally there were three or four measurements per tubule for a given set of experimental conditions. The mean values for individual tubules were then used to calculate a mean value ± standard error of the mean (SE) for the indicated number of tubules. The experimental results were expressed in this manner. When control and experimental observations were made within the same tubule, *P* values for mean paired differences were computed with the Student *t* test by comparing the differences to zero.

## RESULTS

### *Consideration of Prior Data*

Our earlier analysis (31) of fluid absorption coupled to passive salt flows depended heavily on the range of values chosen for the parameter $\alpha$ (cf. below), and on the apparent magnitude of the $Cl^-/HCO_3^-$ selectivity ratio in these tubules. Because these issues have particular relevance to the present studies, the arguments and data will be considered in some detail.

*Parameter $\alpha$.* The transepithelial electrical resistance of these tubules, measured by Lutz et al. (20) when the perfusate and bath contained serum ultrafiltrate and rabbit serum, respectively, is approximately 5 $\Omega$-cm$^2$. And a layer of Krebs-Ringer buffer having a thickness of $7.5 \times 10^{-4}$ cm, i.e., the thickness of the epithelium, has a computed resistance of 0.045 $\Omega \cdot cm^2$ (31). Since passive ion permeation in these tubules may involve an extracellular route (33), we defined a dimensionless parameter $\alpha$, which expresses the ionic diffusion resistance of the epithelium with respect to that of an equivalent thickness of free Krebs-Ringer buffer. For the values cited above, we have (31)

$$1 \leq \alpha \leq 110 \qquad (1)$$

where the limiting values for the parameter $\alpha$ assign all of the resistance to passive transepithelial ion permeation either to junctional complexes, for $\alpha = 1$, or to intercellular spaces, for $\alpha = 110$. The transepithelial ionic permeability coefficient measured at zero volume flow ($P_i$, cm s$^{-1}$, for the *i*-th ion) may be related to the parameter $\alpha$ according to the expression (31)

$$\frac{1}{P_i} = \frac{1}{P_i^j} + \frac{\alpha L}{D_i} \qquad (2)$$

where $P_i^j$ (cm s$^{-1}$) is the permeability coefficient of the *i*-th ion across junctional complexes, $D_i$ (cm$^2$ s$^{-1}$) is the free diffusion coefficient of the *i*-th ion, and L is the measured thickness of the epithelium, $7.5 \times 10^{-4}$ cm (33). The values of $P_i^j$ computed for varying values of $\alpha$ are shown in Table 2. It is evident from these data that for $Na^+$, $HCO_3^-$, and isethionate, virtually all of the resistance to transepithelial passive ion permeation is referable to junctional complexes. For the more permeable $Cl^-$ species, intercellular spaces make a relatively small contribution to the total resistance to $Cl^-$ permeation when $\alpha$ exceeds 25.

As indicated above, a solution (31) of the flow-diffusion equations for lateral intercellular spaces of tubules perfused and bathed at 21°C with Cl-KR and $HCO_3$-KR solutions, respectively, indicated that for $1 \leq \alpha \leq 100$: the $Na^+$, $Cl^-$, and $HCO_3^-$ concentrations in intercellular spaces were uniform as a function of channel length and very nearly in equilibrium with the bathing solutions; and because the intercellular spaces were isosmotic with the external solutions, fluid absorption linked to passive ion absorption could be rationalized entirely in terms of an extracellular rather than a transcellular route.

TABLE 2. *Relationship between $\alpha$ and $P_i^j$*

| $\alpha$ | $P^j_{Na}$ | $P^j_{Cl}$ | $P^j_{HCO_3}$ | $P^j_{Isethionate}$ |
|---|---|---|---|---|
| | | cm sec$^{-1}$ × $10^4$ | | |
| 1 | 0.23 | 0.73 | 0.04 | 0.023 |
| 25 | 0.23 | 0.78 | 0.04 | 0.023 |
| 50 | 0.24 | 0.84 | 0.04 | 0.023 |
| 75 | 0.25 | 0.91 | 0.04 | 0.023 |
| 100 | 0.26 | 1.00 | 0.04 | 0.023 |

The values for $P_i^j$ at $\alpha = 1$ are the previously reported (31, 33) transepithelial ionic permeability coefficients for these tubules, measured at zero volume flow. The values of $P_i^j$ for $\alpha > 1$ were computed from *equation 1* as described previously (31); L was taken to be $7.5 \times 10^{-4}$ cm (31, 33).

Two other results particularly germane to the present paper emerged from the above-mentioned analysis (31). First, dissipative ion transport ($J_i^p$, cm s$^{-1}$ cm$^{-2}$) across junctional complexes of these tubules may be expressed as (16, 17, 31, 35)

$$J_i^p = -P_i^j \left(\Delta C_i^j + \frac{z_i F}{RT} \bar{C}^j \, \Delta V^j\right) + \beta J_v \left(1 - \sigma_i^j\right) \bar{C}_i^j \qquad (3)$$

where $\Delta C_i^j$ and $\Delta V^j$ are, respectively, the concentration difference for the *i*-th ion and the voltage across junctional complexes; $P_i^j$ is the permeability coefficient of the *i*-th ion across junctional complexes, as defined in Table 2; $\beta$ is the fraction of net fluid absorption traversing junctional complexes (as indicated above, $\beta$ is unity for the case of isotonic fluid absorption linked to passive salt absorption); $\sigma_i^j$ is the reflection coefficient of the *i*-th ion across junctional complexes; $\bar{C}_i^j$ is the mean of the *i*-th ion concentrations on either side of the junctional complexes; $z_i$ is the valence of the *i*-th ion; and *R, T,* and *F* have their usual meaning. With measured $J_i^p$, $J_v$, and $V_e$ values, the measured and computed $P_i^j$ values listed in Table 2, and the values computed for $\Delta C_i^j$, $\bar{C}_i^j$, and $\Delta V^i$ from the integrated flow-diffusion equations (cf. above), it was possible (31) to compute $\sigma_i^j$, the ionic reflection coefficient for the *i*-th ion across junctional complexes. Likewise, because fluid absorption linked to passive salt flows may have involved an extracellular route (31), $P_f^j$ (cm s$^{-1}$), the osmotic water permeability of the junctional complexes, was computed from the expression

$$J_v = P_f^j \, \bar{V}_w \sum_{i=1}^{3} \sigma_i^j \, \Delta C_i^j \qquad (4)$$

where $J_v$ (cm$^3$ s$^{-1}$ cm$^{-2}$) is the rate of net volume absorption, $\bar{V}_w$ is the partial molar volume (cm$^3$ mol$^{-1}$) of water, and the summation term refers to $Na^+$, $Cl^-$, and

$HCO_3^-$. Table 3 and Fig. 1 present the values of $\sigma_i^j$ and $P_f^j$, respectively, which were calculated in this manner for varying values of $\alpha$.

Finally, the data in Fig. 1 permit a more explicit evaluation of the range of values for the parameter $\alpha$. An uncertainty arises if the upper limit of $\alpha$ is defined solely in terms of transepithelial resistance data, i.e., according to *equation 1*. For example, the partial conductance ($g_i$, $\Omega^{-1}$ $cm^{-2}$) of the $i$-th ion across a membrane may be expressed as

$$g_i = \frac{F^2}{RT} Z_i^2 P_i [C_i] \tag{5}$$

where $[C_i]$ is the aqueous phase concentration (eq $cm^{-3}$) of the $i$-th ion. With the values of $P_{Na}$ and $P_{Cl}$ computed in this laboratory (33) for these tubules (Table 2), *equation 5* yields $(g_{Na} + g_{Cl}) = 0.042\ \Omega^{-1} \cdot cm^{-2}$, or a transepithelial resistance, due solely to ($Na^+$ + $Cl^-$), of 23.8 $\Omega \cdot cm^2$.

We have no certain explanation for the discrepancy between the electrical resistances measured directly for these tubules by Lutz et al. (20), and the greater resistance value computed from ($P_{Na}$ $P_{Cl}$) according to *equation 5*. In principle, at least three factors, alone or in combination, could account for the phenomenon. First, the resistance measurements of Lutz et al. (20) may have been erroneously low because of an artifactual shunt conductance. But the diameter of the tubule lumen computed electrically by Lutz et al. (20) coincided nearly exactly with the optically measured luminal diameter. In the autoperfused dog kidney, Boulpaep and Seely (3) also measured a proximal tubular electrical resistance of 5.6 $\Omega \cdot cm^2$, with a close agreement between optical and electrical methods of measuring luminal diameter. Second, our isotopic measurements (33) of $P_{Na}$ and $P_{Cl}$ may have been artifactually low. But Kawamura et al. (15) have obtained nearly the same $P_{Na}$ value and a slightly lower $P_{Cl}$ value for isolated rabbit superficial proximal straight tubules; and the $P_{Na}/P_{Cl}$ ratio measured isotopically concides almost exactly with that measured by electrical transference methods (15, 33). Third, an unidentified ion, present in rabbit serum and serum ultrafiltrate but not in artificial mediums, may have contributed to the electrical resistance measured by Lutz et al. (20). In the present context, it is important to note that since *equation 5*, together with ($P_{Na}$ + $P_{Cl}$), yields a higher electrical resistance than measured by Lutz et al. (20), it is evident that our upper limit for $\alpha$ needs assessment by an alternate method.

In this regard, Welling (L. W. Welling, unpublished observations) has measured $P_f^o$, the transepithelial water permeability coefficient of rabbit superficial proximal straight tubules, from net water fluxes produced by hydrostatic pressure gradients, and has obtained a value of 0.2535 ± 0.027 cm $s^{-1}$ (SE; 12 tubules). Figure 1 indicates that only values of $\alpha \leqq 65$ predict $P_f^j$ values $\leqq$ 0.2535 cm $s^{-1}$; indeed, for $\alpha > 65$, $P_f^j$ becomes infinite, and cannot be used for computation. In short, only the restricted range of

$$1 \leq \alpha \leq 65 \tag{6}$$

is consistent simultaneously with the observed rates of fluid absorption coupled to passive salt flows (31), measured transepithelial electrical resistances (20), measured ionic permeability coefficients (33), a measured $P_f^o$ of 0.2535 cm $s^{-1}$, and any finite value of $P_f^j$.

*Value of $P_{HCO_3}$*. To our knowledge, three sets of workers, Warnock and Burg (37), Kawamura et al. (15), and our laboratory (31, 33), have assessed the relative ionic permeability properties of isolated superficial proximal straight tubules. The isotopic values of $P_{Na}$ and $P_{Cl}$ determined in this laboratory (33) and by Kawamura et al. (15) are in close accord with each other, and with the $P_{Na}/P_{Cl}$ ratios estimated from electrical transference methods.

In the case of $HCO_3^-$, in which permeability coefficients have been deduced solely from electrical transference methods, there is a seeming divergence of results. Table 4 indicates that while both Warnock and Burg (37) and our laboratory (31) have measured lumen-posi-

TABLE 3. *Derived values of $\sigma_j^i$ in terms of $\alpha$*

| $\alpha$ | $\sigma^j_{Na}$ | $\sigma^j_{Cl}$ | $\sigma^j_{HCO_3}$ |
|---|---|---|---|
| 1 | 0.9 | 0.78 | 0.97 |
| 25 | 0.95 | 0.83 | 0.97 |
| 50 | 0.96 | 0.88 | 0.97 |
| 75 | 1.0 | 0.95 | 0.97 |

The derived values for $\sigma_i^j$ in terms of $\alpha$ are from Ref. 31, and were computed as described in the text according to *equation 3*.

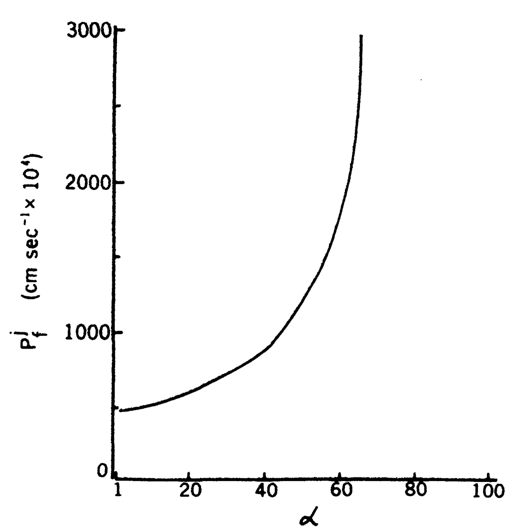


FIG. 1. Relationship between predicted value of $P_f^j$ and $\alpha$. From Table 11 in Ref. 31.

TABLE 4. *Comparison of electrically computed $Cl^-/HCO_3^-$ selectivity ratios*

| Perfusate | | Bath | | Bi-ionic Voltage, mV | $P_{HCO_3}/P_{Cl}$ | $P_{HCO_3}$, μm $sec^{-1}$ | Ref. |
|---|---|---|---|---|---|---|---|
| [Cl], mM | [$HCO_3^-$], mM | [$Cl^-$], mM | [$HCO_3^-$], mM | | | | |
| 150 | 0 | 125 | 25 | 2.1 | 0.35 | 0.2 | 37 |
| 113.6 | 3.8 | 136.4 | 25 | 3.7 | 0.05 | 0.04 | 31 |

The $P_{HCO_3}/P_{Cl}$ ratios and the values for $P_{HCO_3}$ were computed from the bi-ionic voltage (lumen with respect to bath) and isotopic $P_{Na}$ and $P_{Cl}$ data as described in the indicated reference.

tive bi-ionic voltages indicating $P_{HCO_3}/P_{Cl}$ ratios less than unity, the computed $P_{HCO_3}$ values from the two laboratories differ; a $P_{HCO_3}/P_{Cl}$ value of approximately 0.45 may also be computed from the bi-ionic voltage data reported by Kawamura et al. (15).

These differing results may be reconciled in part by noting the steep variation of $P_{HCO_3}$ with slight changes in bi-ionic voltages. For example, the bi-ionic voltage may be expressed according to the Goldman-Hodgkin-Katz equation

$$V_e = \frac{RT}{F} \cdot ln \frac{P_{Na}[Na]^b + P_{Cl}[Cl]^l + P_{HCO_3}[HCO_3]^l}{P_{Na}[NA]^l + P_{Cl}[Cl]^b + P_{HCO_3}[HCO_3]^b} \quad (7)$$

where the superscripts $b$ and $l$ refer to ionic concentrations in the bath and lumen, respectively. For a Cl-KR* perfusate, an $HCO_3$-KR* bath, and $P_{Na}$ and $P_{Cl}$ values of $0.23 \times 10^{-4}$ cm $s^{-1}$ and $0.73 \times 10^{-4}$ cm $s^{-1}$, respectively (Ref. 33 and Table 2), the absolute value of $P_{HCO_3}$ varies strikingly with small changes in $V_e$. A similar result obtains if one carries out these calculations using the Nernst-Planck equation rather than *equation 7*.

Thus, there is qualitative agreement among the results of Kawamura et al. (15), Warnock and Burg (37), and this laboratory (31) that $P_{HCO_3}/P_{Cl}$ is less than unity. But because $P_{HCO_3}$ has not been measured by an independent method, caution should be exercised in assigning an exact value to this coefficient. Accordingly, in the data analyses presented in this paper, we carry out parallel calculations using both of the $P_{HCO_3}$ values listed in Table 4.

*Experimental*

Earlier observations (31) on $J_v$ and $V_e$ in superficial proximal straight tubules exposed to asymmetrical solutions were obtained with Cl-KR perfusates and $HCO_3$-KR bathing mediums, both of which contained acetate (Table 1). Since acetate is actively absorbed from luminal solutions by an as yet unknown mechanism (29), the present experiments assessed the transport characteristics of these tubules in acetate-free asymmetrical solutions.

*Effect of acetate omission on $J_v$.* Table 5 illustrates the effects of acetate omission and cooling on $J_v$. In all instances, $J_v$ measurements were carried out on the same tubule under three randomly varied experimental conditions: at 37°C, when the perfusate and bath contained, respectively, Cl-KR and $HCO_3$-KR buffer; and at either 21° or 37°C, when the perfusate and bath contained, respectively, Cl-KR* and $HCO_3$-KR* buffers. At 37°C, $J_v$ was not significantly affected when acetate in both the perfusing and bathing mediums was replaced by isethionate. And in acetate-free mediums, cooling from 37° to 21°C resulted in approximately a 60% reduction in $J_v$. In earlier studies with a Cl-KR perfusate and an $HCO_3$-KR bath, either ouabain or cooling reduced $J_v$ by 52–60% (31); thus, the rate of fluid absorption linked to the dissipative salt transport which occurs when these tubules are exposed to asymmetrical salt solutions was nearly the same, with or without acetate. (As noted previously [31], $J_v$ at 21°C in the presence of asymmetrical solutions, e.g., Table 5, is referable to oppositely directed $Cl^-$ and $HCO_3^-$ concentration gradients, and not to oppositely directed concentration gradients for urea and alanine plus glucose.)

*Effect of varying temperature on $V_e$.* With a Cl-KR perfusate and an $HCO_3$-KR bath, $V_e$ is lumen-positive at 37°C in the range +2.8–3.2 mV, and rises approximately 0.4–0.7 mV when active transport is inhibited either by cooling to 21°C or by addition of $10^{-4}$ M ouabain to the bath (31). Because $V_e$ evidently contributes to the electrochemical gradient for transepithelial $Na^+$ and $Cl^-$ transport, it was relevant to assess $V_e$ at 37°C in acetate-free asymmetrical solutions and the effect of cooling on $V_e$. Figure 2 and Table 6 illustrate that when the tubules were perfused and bathed with, respectively, Cl-KR* and $HCO_3$-KR* buffers, $V_e$ was approximately +3.7 mV lumen positive at 21°C. Warming to 37°C resulted in approximately a 1.0 mV decrement in $V_e$, which was reversed by cooling again to 21°C. We

TABLE 5. *Effects of acetate omission and cooling on fluid absorption*

| Perfusate | Bath | T, °C | $J_v$ (nl $min^{-1}$ $mm^1$) | $\Delta J_v$ (nl $min^{-1}$ $mm^1$) |
|---|---|---|---|---|
| Cl-KR | $HCO_3$-KR | 37 | 0.41 ± 0.04 | |
| | | | | 0.01 ± 0.01 ($P > 0.05$) |
| Cl-KR* | $HCO_3$-KR* | 37 | 0.39 ± 0.03 | |
| | | | | 0.23 ± 0.03 ($P < 0.02$) |
| Cl-KR* | $HCO_3$-KR* | 21 | 0.16 ± 0.01 | |

$J_v$ was measured under the indicated conditions in each of 6 tubules. The order in which $J_v$ measurements were made varied randomly among the individual tubules.

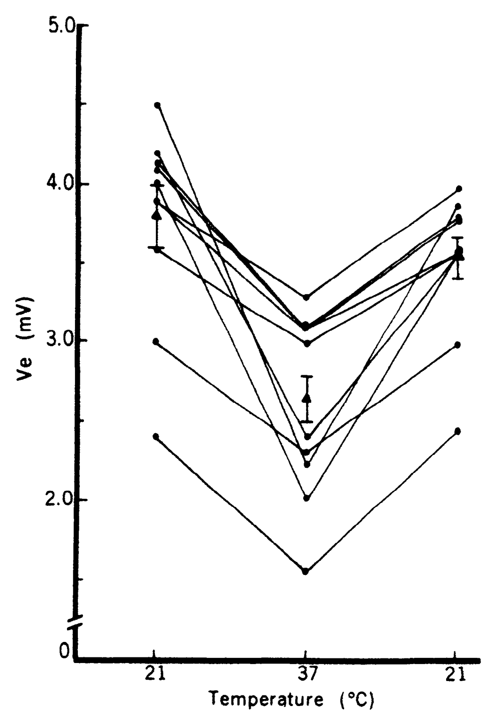


FIG. 2. Effect of cooling on $V_e$. Perfusate contained Cl-KR* and bath contained $HCO_3$-KR*. In each tubule, $V_e$ was measured first at 21°, then at 37°, and lastly at 21°C. Lines connect measurements on same tubule.

conclude that for these conditions, institution of active $Na^+$ absorption was accompanied by a clearly discernible fall in $V_e$.

*Net $Cl^-$ absorption at 37°C.* In the case of fluid absorption from superficial proximal straight tubules exposed to symmetrical $HCO_3$-KR solutions at 37°C, $Cl^-$ is the counterion for approximately 25% of absorbed $Na^+$ (29, 33). In the case of passive salt absorption from acetate-containing asymmetrical solutions (a Cl-KR perfusate and an $HCO_3$-KR bath), $Cl^-$ is the sole anion in an isotonic fluid absorbate (31). Table 7 presents an assessment of net $Cl^-$ absorption from acetate-free asymmetrical solutions at 37°C.

The perfusate and bath contained, respectively, Cl-KR* and $HCO_3$-KR*, and the system was maintained at 37°C. Net $Cl^-$ flux was computed from chemical balances. Since net lumen-to-bath $Na^+$ flux accounts quantitatively for isotonic fluid transport in these tubules, either at 37° or at 21°C (29, 31, 33), the predicted net cation absorption rate ($J_{cation}$) in Table 7 was computed from $J_v$ for the case of an isotonic salt absorbate. Table 7 illustrates clearly that the $Cl^-$ concentration of collected fluid was virtually indistinguishable ($P > 0.2$) from that of the perfusate, and that $Cl^-$ was the counterion for approximately 85% of cation, i.e., $Na^+$, absorption.

## *Analytical*

We now consider a model for evaluating fluid absorption linked to active plus passive ion transport processes when these tubules were exposed to asymmetrical acetate-free KR solutions. In these tubules, net $Na^+$ absorption accounts quantitatively for isotonic fluid transport when the tubules are perfused and bathed with symmetrical $HCO_3$-KR solutions, and fluid absorption is linked to active plus passive net $Na^+$ flux (29, 33), and when the perfusate and bath contain, respectively, Cl-KR and $HCO_3$-KR buffers, and fluid absorption is linked to dissipative $Na^+$ flux (31). Likewise, $Na^+$ absorption is an isotonic process in isolated proximal convoluted tubules (4, 18).

Alternatively, Sackin and Boulpaep (26) have recently proposed that in proximal convolutions of *Necturus* absorbed fluid may be slightly (e.g., approximately 2 mM) hypertonic to luminal fluids. Clearly, such a degree of hypertonicity could not be detected in isolated perfused tubules given currently available methodology. Moreover, these workers (26) also considered the possibility of osmotic equilibration of tubular fluid with interstitial fluid, followed by final fluid transport into peritubular capillaries. The experimental data in the present paper do not permit such an evaluation.

The present analysis will, therefore, consider the case of isotonic fluid absorption from these tubules when the perfusate and bath contain, respectively, Cl-KR* and $HCO_3$-KR* buffers, both at 37°C. The aqueous phases are taken as containing three ions: $Na^+ = 1$; $Cl^- = 2$; and $HCO_3^- = 3$. The experimental data to be analyzed are $J_v$, $J_1$, $J_2$, $J_3$, and $V_e$, and these values, obtained from Tables 5–7, are summarized in Table 8.

*Model.* The analytical model, illustrated schematically in Fig. 3, includes a component identical to that presented previously (31), and also considers terms for active ion transport. An unstirred channel lacking fixed charges and having an unspecified geometry separates the luminal and bathing solutions, and is bounded laterally by a cellular compartment; 1 $cm^2$ of luminal membrane contains $n$ channels. Each channel is separated from the lumen by a membrane (the junctional complex) at $x = 0$, and from the bath by a membrane (the peritubular basement membrane) at $x = L$. The concentrations (eq $cm^{-3}$) of the $i$-th ion in lumen, cell, channel, and bath are designated as, respectively, $C_i^l$, $C_i^c$, $C_i^x$, and $C_i^b$. All ion and volume flows are taken as positive in the direction of increasing x.

Volume flow may enter the $k$-th channel either through an extracellular route ($j_v^e$) or through a cellular route ($j_v^c$), and all of the transported fluid, designated $j_v^L$, leaves the channel at $x = L$. Ions may enter the channel through an extracellular route ($j_i^e$) or through a

TABLE 6. *Effect of cooling on transepithelial voltage*

| T, °C | $V_e$, mV | $\Delta V_e$, mV |
|---|---|---|
| 21 | 3.8 ± 0.2 | |
| | | 1.1 ± 0.2 ($P < 0.001$) |
| 37 | 2.7 ± 0.2 | |
| | | 0.9 ± 0.1 ($P < 0.001$) |
| 21 | 3.6 ± 0.1 | |

This table presents the mean values ± SE for the data shown in Fig. 3. $n$, 10.

TABLE 7. *Chloride absorption at 37°C with acetate-free mediums*

| Tubule, mm | Perfusate | | Collected Fluid | | $J_v$, nl min$^{-1}$ mm$^{-1}$ | $J_{Cl}$ | $J_{cation}$ | $J_{Cl}/J_{cation}$, % |
|---|---|---|---|---|---|---|---|---|
| | [$Cl^-$], mM | Rate, nl min$^{-1}$ | [$Cl^-$], mM | Rate, nl min$^{-1}$ | | eq min$^{-1}$ mm$^{-1}$ × $10^{11}$ | | |
| 3.60 | 139.9 | 12.32 | 139.4 | 10.88 | 0.40 | 5.74 | 6.23 | 92.0 |
| 2.85 | 138.8 | 11.97 | 139.8 | 10.94 | 0.36 | 4.66 | 5.61 | 83.0 |
| 3.5 | 138.8 | 11.18 | 137.6 | 9.93 | 0.36 | 5.30 | 5.61 | 94.0 |
| 3.45 | 138.8 | 10.10 | 137.8 | 9.00 | 0.39 | 4.32 | 6.08 | 71.0 |
| 3.4 | 137.9 | 9.18 | 137.8 | 7.66 | 0.45 | 6.20 | 7.01 | 88.0 |
| 3.2 | 137.9 | 11.28 | 139.3 | 9.73 | 0.48 | 6.25 | 7.48 | 84.0 |
| Mean | 138.7 | | 138.6 | | 0.41 | 5.41 | 6.39 | 85.3 |
| ±SE | ±0.3 | | ±0.3 | | ±0.05 | ±0.33 | ±0.32 | ±3.4 |

The perfusate and bath contained, respectively, Cl-KR* and $HCO_3$-KR* buffer. $J_{Cl}$, the net rate of $Cl^-$ absorption, was computed from the $Cl^-$ concentration in the perfusate and collected fluid, and the perfusing and collection rates. $J_v$ was measured as described in METHODS. $J_{cation}$ was computed from $J_v$ for the case of isotonic fluid absorption (29, 31, 33).

TABLE 8. *Experimental data for analysis*

| Data | Source |
|---|---|
| $J_v = 9.76 \times 10^{-6}\ cm^3\ s^{-1}\ cm^{-2}$ | Table 7 |
| $J_1 = 1.52 \times 10^{-9}$ eq $s^{-1}\ cm^{-2}$ | Table 7 |
| $J_2 = 1.29 \times 10^{-9}$ eq $s^{-1}\ cm^{-2}$ | Table 7 |
| $J_3 = 0.23 \times 10^{-9}$ eq $s^{-1}\ cm^{-2}$ | $(J_1 - J_2)$ |
| $V_e = +2.7$ mV | Table 6 |

cellular route ($j_i^c$); all of the ion flux, designated $j_i^L$, leaves the channel at x = L.

*Assumptions.* Following our previous analysis (31), we set the following assumptions.

*1)* The channels are considered uniform, i.e., the geometric and frictional constraints to diffusion and convection, the loci of active ion transport, and the rate of active ion transport, are the same within all channels (31). Thus, $J_i$, the net flux of the *i*-th ion for 1 $cm^2$ of membrane area, is

$$J_i = \sum_{k=1}^{n} j_i^L \tag{8a}$$

and $J_v$, the net volume flow for 1 $cm^2$ of membrane area, is

$$J_v = \sum_{k=1}^{n} j_v^L \tag{8b}$$

*2)* The dimensionless parameter $\alpha$ (31), within the range defined in *equation 6,* is considered as providing an estimate of the diffusion resistance of intercellular spaces, exclusive of junctional complexes, with respect to a layer of free solution having the same thickness as the epithelium. We emphasize again in this regard that the upper limit of 65 for $\alpha$ has been set using hydraulic conductivity comparisons between computed and observed values (Fig. 1 and Ref. 31), and not by electrical resistance measurements.

*3)* Passive ion permeation in these tubules may involve an extracellular route, so it is likely that junctional complexes are appreciably more permeable to ions than lateral or basilar membranes (31, 33). Thus, as in the standing gradient model (9), we consider the membranes separating the cellular and channel compartments to have unity reflection coefficients for $Na^+$, $Cl^-$, and $HCO_3^-$ (31).

*4)* Welling et al. (39) have noted that peritubular basement membranes of superficial proximal straight tubules are very permeable to water, particularly with respect to luminal surfaces, and moderately permeable to albumin. Accordingly, we assume a zero reflection coefficient for $Na^+$, $Cl^-$, and $HCO_3^-$ at x = L, i.e., we assume that $C_i^L = C_i^b$ (31). Since the hydraulic conductivity of peritubular capillary basement membranes in these tubules exceeds $4 \times 10^{-2}$ cm $s^{-1}$ $atm^{-1}$ (39), one requires a negligible pressure gradient, e.g., 0.1–0.2 $cmH_2O$, to account for volume flow between intercellular spaces and bath. Consequently, hydrostatic pressure terms will not be considered in the present analysis.

*5)* The dissipative permeability characteristics of junctional complexes, listed in Tables 2 and 3 for varying values of $\alpha$, will be utilized. As indicated above, two

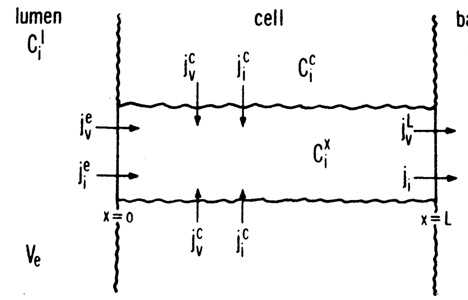


FIG. 3. Schematic diagram of model for evaluating fluid absorption linked to active plus passive ion flows.

values for $P_{HCO_3}$ will be used: $P_{HCO_3} = 0.04 \times 10^{-4}$ cm $s^{-1}$, as obtained in this laboratory (31) (Table 4); and $P_{HCO_3} = 0.2 \times 10^{-4}$ cm $s^{-1}$, as obtained by Warnock and Burg (37) (Table 4).

*6)* The cells are considered to be in osmotic equilibrium with the external solutions. Since a unity reflection coefficient has been assigned for $Na^+$, $Cl^-$, and $HCO_3^-$ across the membranes separating cellular and channel compartments, the total cellular ion content is taken to be twice the cation content of the external solutions.

*Flow-diffusion equations.* For uniform channels, the flux of the *i*-th ion through a plane at x normal to the direction of solute transport is, for 1 $cm^2$ of luminal surface area (31)

$$J_i^x = -\frac{D_i}{\alpha}\left[\frac{d\,C_i^x}{dx} + \frac{z_i F}{RT} C_i^x \frac{dV^x}{dx}\right] + J_v^x C_i^x \tag{9}$$

where $J_v^x$ is the net volume flux crossing x for 1 $cm^2$ of luminal surface area, and $V^x$ is the voltage at x. The electroneutrality condition is

$$C_1^x = C_2^x + C_3^x \tag{10}$$

*Equations 9* and *10* may be solved simultaneously to yield

$$\frac{d\,C_1^x}{dx} = \frac{1}{2}\left\{\left(\frac{\alpha}{D_1} + \frac{\alpha}{D_3}\right)(J_v^x C_1^x - J_1^x) + \left(\frac{\alpha}{D_2} - \frac{\alpha}{D_3}\right)(J_v^x C_2^x - J_2^x)\right\} \tag{11}$$

$$\frac{d\,C_2^x}{dx} = \frac{1}{2}\left\{\left(\frac{\alpha}{D_1} - \frac{\alpha}{D_3}\right)(J_v^x C_1^x - J_1^x)\frac{C_2^x}{C_1^x} + \left[\frac{2\alpha}{D_2} - \left(\frac{\alpha}{D_2} - \frac{\alpha}{D_3}\right)\frac{C_2^x}{C_1^x}\right](J_v^x C_2^x - J_2^x)\right\} \tag{12}$$

and

$$\frac{dV^x}{dx} = \frac{RT}{F}\left[\frac{J_v^x\,\alpha}{D_1} - \frac{1}{C_1^x}\frac{d\,C_1^x}{dx} - \frac{J_1^x\,\alpha}{D_1\,C_1^x}\right] \tag{13}$$

*Equations 9–13* are identical to those presented elsewhere (31) for fluid absorption linked to passive ion flows which occur in these tubules.

We now consider the expressions for the gradient of volume flow and the gradient of ion flow. As defined previously (31), the gradient of volume flow is

$$\frac{d\,J_v^x}{dx} = P_f^{c\prime}\,\bar{V}_w\left[\sum_{i=1}^{3}(C_i^x - C_i^c)\right] \tag{14}$$

where $P_f^{c\prime}$ ($s^{-1}$), the osmotic water permeability coefficient per unit channel length for the membrane separating cellular and space compartments, is

$$P_f^{c\prime} = \frac{P_f^c}{L} \tag{15}$$

where $P_f^c$ is the osmotic water permeability coefficient (cm $s^{-1}$) of the membrane between cells and channel. Clearly, $P_f^c$ is not known directly. But since all volume flow is considered to enter the channels through either a cellular or a paracellular route, and since all volume flow is considered to exit the channels at x = L, we may express $P_f^c$ as

$$P_f^c = P_f^o - P_f^j \tag{16}$$

where $P_f^o$ is the observed transepithelial water conductance (cf. above; $P_f^o = 0.2535 \pm 0.027$ cm $s^{-1}$). By substituting this value for $P_f^c$ in *equation 16*, and substituting the latter in *equation 15*, we have

$$P_f^{c\prime} = \frac{0.2535 - P_f^j}{L} \tag{17}$$

where $L = 7.5 \times 10^{-4}$ cm (31, 33) and $P_f^j$, for varying values of $\alpha$, may be obtained from Fig. 1. We emphasize again in this regard that the values of $P_f^j$ in Fig. 1 were obtained (cf. Ref. 31) for the case of fluid absorption traversing an extracellular route.

To evaluate the gradient for ion flow, we note that for combined active plus passive ion flows $J_i^x$ may be expressed as

$$J_i^x = J_i^p + \tau_i\,(N_i - M_i) \tag{18}$$

where $J_i^p$ is the passive component of the *i*-th ion flux crossing x in 1 cm² of luminal surface area ($J_i^p$ is assumed to enter the channels at x = 0 via an extracellular route), $\tau_i$ is the rate of active transport (eq/s·cm of channel length) of the *i*-th ion in 1 cm² of luminal surface area, and $M_i$ and $N_i$ are, respectively, the beginning and end of the sites along the channel length for active transport of the *i*-th ion in the x direction. Accordingly we have

$$\tau_i = 0 \text{ for } \left\{\begin{matrix} 0 \le x < M_i \\ N_i < x \le L \end{matrix}\right\} \tag{19}$$

and the gradient of ion flux is

$$\frac{d\,J_i^x}{dx} = \tau_i \tag{20}$$

Thus, we may define $J_i^a$ (eq $s^{-1}$ $cm^{-2}$), the net rate of active ion absorption, as

$$J_i^a = \tau_i\,(N_i - M_i) \tag{21}$$

*An approximation solution for the model.* It is clear from *equations 20* and *21* that computation of the solute concentration profiles in intercellular spaces requires an assessment of $J_i^a$. To our knowledge, there exists no explicit method for evaluating this term. But it may be possible to obtain a reasonable estimate of $J_i^p$, the rate of net passive ion absorption, and then to obtain $J_i^a$ as the difference between $J_i$ and $J_i^p$ by expressing *equation 3* in terms of transepithelial driving forces

$$J_i^p \simeq -P_i\left\{(C_i^b - C_i^l) + \frac{z_i F}{RT}\left(\frac{C_i^l + C_i^b}{2}\right)V_e\right\} + J_v\,(1 - \sigma_i^j)\left(\frac{C_i^l + C_i^b}{2}\right) \tag{22}$$

i.e., where $P_i$ (Table 2, and for $P_{HCO_3}$ also Table 4) and $\sigma_i^j$ (Table 3) are for $\alpha = 1$.

The use of *equation 22* to approximate $J_i^p$ in these tubules may be justified, at least as a reasonable choice, by a number of considerations. There are at least three instances in which *equation 22* has described adequately the measured rates of net passive ion transport in these tubules. These include net passive $Cl^-$ absorption from tubules perfused and bathed with symmetrical $HCO_3$-KR solutions at 37°C, i.e., during combined active and passive net ion transport (29); and net passive $Na^+$ and $Cl^-$ absorption from tubules perfused and bathed at 21°C with, respectively, Cl-KR and $HCO_3$-KR solutions, i.e., during fluid absorption coupled to passive ion transport (31).

In all of the above situations, diffusion has comprised 75–100% of net passive ion flux (29, 31), in accord with the fact that the $\sigma_i^j$ values listed in Table 3 are close to unity. And Table 2 indicates that for the range $1 \le \alpha \le 65$ (cf. *equation 6*), junctional complexes constitute either the major (for $Cl^-$) or sole (for $Na^+$ and $HCO_3^-$) resistance for transepithelial ionic diffusion. So it may be that the intercellular spaces are very nearly in diffusion equilibrium with the bathing solutions. Indeed, the latter description applies to the case of fluid absorption linked to passive NaCl flux in these tubules (31).

Based on these empirical and theoretical observations, we argue that for these tubules *equation 22* provides a reasonable method for assessing $J_i^p$. Stated in another way, we assume that $C_i^o$, the concentration of the *i*-th ion at x = 0, is virtually the same as $C_i^b$, the concentration of the *i*-th ion in the bath; and that $V_e$, the transepithelial voltage, is virtually the same as the voltage across junctional complexes. It is important to note in this context that the use of *equation 22* does not imply that the actual value of $\alpha$ is unity, but rather that because the values of $P_i^j$ (Table 2) and $\sigma_i^j$ (Table 3) vary only slightly for $1 \le \alpha \le 65$, the use of *equation 22* provides a reasonable way of approximating the magnitude of passive ion transport.

The argument may have a more general applicability to passive ion transport in mammalian proximal renal tubules. Sauer (27) has deduced from thermodynamic considerations that an expression formally identical to *equation 22* may be used to assess passive ion transport in renal tubules. And Frömter et al. (10), Ullrich (35), and Neumann and Rector (23) have used the equivalent of *equation 22* to describe the passive components of ionic fluxes measured during in vivo micropuncture of rat proximal convolutions.

Table 9 lists the values of $J_i^p$, and the diffusion and

TABLE 9. *Contributions of active and passive transport processes to net ion absorption*

| Ion | $J_i$ | Total $J_i^p$ | Diffusion | Solvent Drag | $J_i^a$ |
|---|---|---|---|---|---|
| | | eq sec$^{-1}$ cm$^{-2}$ × 10$^9$ | | | |
| $Na^+$ | 1.52 | 0.51 | 0.36 | 0.15 | 1.01 |
| $Cl^-$ | 1.28 | 1.20 | 0.93 | 0.27 | |
| Using $P_{HCO_3}$ = 0.04 × 10$^{-4}$ cm s$^{-1}$ | | | | | |
| $HCO_3^-$ | 0.24 | −0.103 | −0.11 | 0.008 | 0.34 |
| Using $P_{HCO_3}$ = 0.20 × 10$^{-4}$ cm s$^{-1}$ | | | | | |
| $HCO_3^-$ | 0.24 | −0.582 | −0.59 | 0.008 | 0.82 |

The values of $J_i$ are from Table 8. $J_i^p$, the net passive flux of the *i*-th ion, and the diffusional and entrained components of this flux, were computed according to *equation 22* from $J_i$. For $Na^+$ and $Cl^-$, $P_i$ and $\sigma_i^j$ were taken from Tables 2 and 3, respectively; $\sigma^j_{HCO_3}$ was taken from Table 3; the two indicated values of $P_{HCO_3}$ were used. A negative sign denotes bath-to-lumen flux.

solvent drag components of $J_i^p$, which were computed according to *equation 22;* and the values of $J_i^a$, computed as the difference between $J_i$ and $J_i^p$. Table 9 indicates that 34% of net $Na^+$ absorption could be accounted for in terms of passive transport processes, in close accord with the experimental observation that for these conditions 41% of net fluid absorption was insensitive to cooling (Table 5). Approximately 70% of passive $Na^+$ transport was diffusional. Net $Cl^-$ transport in these tubules (29), as in the proximal convoluted tubule of the rat (10, 35), is passive. Table 9 shows that within experimental error *equation 22* accounted for net $Cl^-$ absorption. Finally, Table 9 illustrates that, depending on the value of $P_{HCO_3}$ chosen, $J^a_{HCO_3}$ varied. The net effect of assigning the higher value of 0.2 × 10$^{-4}$ cm s$^{-1}$ to $P_{HCO_3}$ was to increase the diffusional backleak of $HCO_3^-$ into the lumen, and, hence, $J^a_{HCO_3}$. For these conditions, the calculated net rate of active $HCO_3^-$ transport was approximately 80% of the net rate of active $Na^+$ transport.

*Solution of flow-diffusion equations*. We may also use numerical integration of the flow-diffusion equations to evaluate the applicability of *equation 22*. *Equations 11–14* and *20* may be integrated numerically (31, 34), subject to the boundary conditions defined in *equations 3, 4,* and *10*. The required inputs are: $C_i^1$, $C_i^b$, and $D_i$; $P_i^j$ in terms of the variable parameter $\alpha$ (Table 2 and, in the case of $HCO_3^-$, also Table 4); $J_i$, $J_v$, and $V_e$ (Table 8); $P_f^{c'}$, in terms of the varying parameter $\alpha$ (*equations 15–17* and Fig. 1); and $\tau_i$, in terms of the varying parameters $N_i$ and $M_i$ (*equations 18, 19,* and *21* and Table 9). The varying parameters are $\alpha$, as defined in *equation 6*, and $(N_i - M_i)$, as defined in *equation 21*.

The solution of *equations 11–14* and *20* yields: $C_i^0$, the concentration of the *i*-th ion at x = 0, $\sigma_i^j$, and $\Delta V^j$. Since *equation 22* equates $C_i^b$ and $V_e$ with, respectively, $C_i^0$ and $\Delta V^j$ in *equation 3,* the solution of *equations 11–14* and *20* provides a way of evaluating the validity of this assumption. And yet another means for testing the applicability of *equation 22* obtains by comparing the $\sigma_i^j$ values used in *equation 22* (i.e., those listed in Table 3) with those obtained from the solution of *equations 11–14* and *20*.

Figure 4 illustrates the values of $(C_i^0 - C_i^b)$ for $1 \leq \alpha \leq 60$, which were computed from numerical integration of *equations 11–14* and *20*. The values of $J_i^a$ were obtained from Table 9 with the value of $P_{HCO_3}$ = 0.04 × 10$^{-4}$ cm s$^{-1}$. When the value of $P_{HCO_3}$ = 0.2 × 10$^{-4}$ cm s$^{-1}$ was used, $C_i^0$ for $Na^+$, $Cl^-$, and $HCO_3^-$ varied by less than 0.01 mM from the $C_i^0$ values shown in Fig. 4. In short, virtually identical values for $C_i^0$ were obtained with the higher and lower values for $P_{HCO_3}$.

It is evident from Fig. 4 that $C^0_{Na}$, $C^0_{Cl}$, and $C^0_{HCO_3}$ were virtually the same as, respectively, $C^b_{Na}$, $C^b_{Cl}$, and $C^b_{HCO_3}$. Further, although the results are not shown in Fig. 4, the concentration of each of the three ions was invariant with x in the interval $0 \leq x \leq 7.5 \times 10^{-4}$ cm. Nearly identical results were obtained when the $J_i^a$ values in Table 9 were used, but for both $Na^+$ and $HCO_3^-$, the interval $M_i$ to $N_i$ in *equation 21* was taken to be from zero to 0.2 × 10$^{-4}$ cm, i.e., when the active transport sites were localized to the apical ends of intercellular spaces.

Thus, for these combinations the intercellular spaces were in virtual equilibrium with the bathing solutions, and varying $P_{HCO_3}$ between 0.04 × 10$^{-4}$ cm s$^{-1}$ and 0.2 × 10$^{-4}$ cm s$^{-1}$ had essentially no effect on $C_i^0$. Evidently, these results are entirely consistent with the use of *equation 22* as a valid approximation for estimating $J_i^p$. It also follows directly that, since the intercellular spaces were isosmotic with the external solutions, net fluid absorption involved an extracellular rather than a transcellular route.

Finally, Table 10 lists the values of $\sigma_i^j$ and $\Delta V_j$ which were computed from numerical integration of *equations 11–14* and *20* for the conditions listed in Fig. 3, and for the case in which $P_{HCO_3}$ was taken to be 0.2 × 10$^{-4}$ cm s$^{-1}$. The computed values of $\Delta V^j$ were virtually identical to the experimentally measured transepithelial voltages (Table 8), and the values of $\sigma_i^j$ computed from the present analysis were virtually the same with the two different values of $P_{HCO_3}$. The $\sigma_i^j$ values in Table 10 were similar to those computed in our earlier studies (Table 3); but, importantly, the computed magnitude of $(\sigma^j_{HCO_3}$

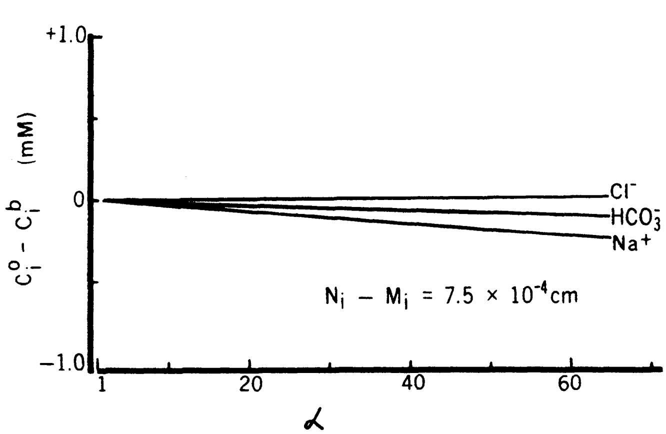


FIG. 4. Values of the differences between solute concentrations at the closed ends of lateral spaces and in 1 bathing solution $(C_i^0 - C_i^b)$ in terms of parameter $\alpha$, computed from numerical integration of *equations 11–14*, and *17*. Values of $J_i$ and $J_i^a$ were taken from Table 9. $N_i - M_i$ in *equation 21* was taken to be 7.5 × 10$^{-4}$ cm, the lateral space length.

TABLE 10. *Values of $\sigma_i^j$ and $\Delta V_i$ corresponding to $C_i^j$*

| $\alpha$ | $\sigma^j_{Na}$ | $\sigma^j_{Cl}$ | $\sigma_{HCO_3}$ | $\Delta V^j$, mV |
|---|---|---|---|---|
| | Using $P_{HCO_3} = 0.04 \times 10^{-4}$ cm $s^{-1}$ | | | |
| 1 | .91 | .65 | .96 | 2.70 |
| 20 | .92 | .70 | .97 | 2.72 |
| 40 | .97 | .75 | .97 | 2.76 |
| 60 | .98 | .86 | .98 | 2.80 |
| | Using $P_{HCO_3} = 0.20 \times 10^{-4}$ cm $s^{-1}$ | | | |
| 1 | .91 | .65 | .95 | 2.69 |
| 20 | .92 | .70 | .98 | 2.69 |
| 40 | .94 | .75 | .99 | 2.69 |
| 60 | .97 | .85 | 1.02 | 2.70 |

The values of $\sigma_i^j$ and $V_e$ were computed for the conditions listed in Fig. 3, with each of the indicated values of $P_{HCO_3}$ and the corresponding transport rates for $HCO_3^-$ from Table 9.

$- \sigma^j_{Cl}$) for a given value of $\alpha$ was greater at 37° (Table 10) than at 21°C (Table 3).

In short, given the measured hydraulic conductivity of these tubules, one can account for isotonic fluid absorption from asymmetrical solutions (i.e., a Cl-KR* perfusate and an $HCO_3$-KR* bath) on the basis of unequal reflection coefficients for $Cl^-$ and $HCO_3^-$, whether a lower ($0.04 \times 10^{-4}$ cm $s^{-1}$) or higher ($0.2 \times 10^{-4}$ cm $s^{-1}$) $P_{HCO_3}$ is chosen. Moreover, when the interval $M_i$ to $N_i$ was taken to be from zero to $0.2 \times 10^{-4}$ cm for both $Na^+$ and $HCO_3^-$, solution of the flow-diffusion equations yielded nonreal values for $\sigma^j_{HCO_3}$. Thus, in terms of the present model, localization of the active transport sites for $Na^+$ and $HCO_3^-$ to the apical ends of intercellular spaces is an unlikely possibility.

## DISCUSSION

The experiments reported in this paper were intended to evaluate ion transport processes and coupled fluid transport in superficial proximal straight tubules exposed to asymmetrical, acetate-free solutions similar in composition to those which might be seen in this nephron segment in vivo. When the tubules were perfused and bathed with, respectively, Cl-KR and $HCO_3$-KR solutions, omission of acetate from both the perfusing and bathing solutions had no significant effect on the rate of fluid absorption (Table 5). When the tubules were perfused and bathed with, respectively, Cl-KR* and $HCO_3$-KR* solutions there was a 60% reduction in net fluid absorption when active $Na^+$ transport was inhibited by cooling (Table 5), and the transepithelial voltage, 2.7 mV, lumen positive at 37°C, rose approximately 1.0 mV when the system was cooled (Fig. 2 and Table 6). These results are very similar to those measured previously (31) when the tubules were exposed to acetate-containing asymmetrical solutions, i.e., a Cl-KR perfusate and an $HCO_3$-KR bath. Finally, net $Cl^-$ absorption accounted for 85% of net cation absorption at 37°C with acetate-free asymmetrical solutions (Table 7).

The analytical model (Fig. 3) was designed to assess the mechanisms of ion and fluid absorption from tubules exposed to asymmetrical, acetate-free solutions at 37°C, with particular regard to the use of *equation 22* in a quantitative assessment of passive ion transport and the driving forces for net fluid absorption. Given the remarkably high hydraulic conductivity of peritubular basement membranes measured for these tubules by Welling and Grantham (39), e.g., in excess of $4 \times 10^{-2}$ cm $s^{-1}$ $atm^{-1}$, and the assumption that those membranes have a zero reflection coefficient for $Na^+$, $Cl^-$, and $HCO_3^-$ (cf. *assumption 4* of the analytical model), a negligible hydrostatic pressure gradient is required to account for the transport of solutes and water from intercellular spaces to bath.

### *Ion Transport: Passive and Active Components*

The results in Table 2 indicate that junctional complexes rather than intercellular spaces constitute most or all of the transepithelial resistance to ionic diffusion. Accordingly, *equation 22* described passive ion transport across junctional complexes in terms of bulk phase driving forces. In empirical terms, there was reasonable agreement between the values for $J_i^p$ predicted from *equation 22* and the experimental data. The net passive $Na^+$ flux predicted from *equation 22* amounted to 34% of total $Na^+$ flux (Table 9), in close accord with the fact that 41% of fluid absorption from these tubules depended on passive transport processes (Table 5). $Cl^-$ transport in these tubules is passive (29), and the net $Cl^-$ flux predicted from *equation 22* was the same, within experimental error, as the measured rate of net $Cl^-$ absorption (Tables 7 and 9). In the case of $HCO_3^-$, the Cl-KR* perfusate and an $HCO_3$-KR* bath produced an electrochemical gradient for passive $HCO_3^-$ backflux from bath to lumen. The magnitude of the computed backflux varied depending on the value of $P_{HCO_3}$ chosen, as did the rate of active $HCO_3^-$ transport required to account for net $HCO_3^-$ absorption. At $P_{HCO_3} = 0.2 \times 10^{-4}$ cm $s^{-1}$ the rate of active $HCO_3^-$ transport was approximately 80% of the rate of active $Na^+$ transport (Table 9).

In order to evaluate these data further, the active and passive ion transport rates computed from *equation 22* were used as variable input parameters into the formal solution of the flow-diffusion equations, which yielded $C_i^0$, $\sigma_j^j$, and $\Delta V^j$. We emphasize again in this regard that the upper limit of 65 for the parameter $\alpha$ depended on hydraulic conductivity considerations. Our earlier analysis of fluid absorption coupled to dissipative salt flows yielded an indeterminate $P_f^j$ value when $\alpha$ exceeded 65 (Fig. 1 and Ref. 31); likewise, only values of $\alpha \leq 65$ were consistent with the transepithelial hydraulic conductivity of 0.2535 cm $s^{-1}$. Further, because of uncertainty concerning the exact value of $P_{HCO_3}$, the computations were carried out with two different $P_{HCO_3}$ values, $0.04 \times 10^{-4}$ cm $s^{-1}$ and $0.2 \times 10^{-4}$ cm $s^{-1}$ (cf. Table 4).

There was also a convergence of the results obtained from *equation 22* with those predicted from the flow-diffusion equations. When the $J_i$, $J_i^p$, and $J_i^a$ values in Table 9 (which were obtained from the experimental data and *equation 22*) were used with the integrated forms of *equations 11–14*, and *20*, the computed concentrations of $Na^+$, $Cl^-$, and $HCO_3^-$ in intercellular spaces (Fig. 3) were virtually identical to those in the bathing solutions. The predicted values for $\sigma_i^j$ (Table 10) were very similar to those used in *equation 22* (Table 3), and the predicted $\Delta V^j$ (Table 10) was virtually the same as the measured $V_e$ (Table 6). Moreover, the values of $C_i^0$, $\sigma_i^j$, and $\Delta V^j$ predicted from the flow-diffusion equations were essentially the same for $P_{HCO_3} = 0.04 \times 10^{-4}$ cm s$^{-1}$ and $P_{HCO_3} = 0.20 \times 10^{-4}$ cm s$^{-1}$.

Taken together, these observations are consistent with the possibility that *equation 22* and the results listed in Table 9 provided a reasonable estimate of the magnitudes of active and passive ion transport in these tubules, at least for the case of a Cl–KR* perfusate and an $HCO_3$–KR* bath. It is relevant to note in this regard that Frömter et al. (10), Ullrich (35), and Neumann and Rector (23) utilized a form of *equation 22* to assess both the amount of passive ion transport and the relative magnitudes of ion diffusion and ion entrainment with solvent flow occurring during fluid absorption in the in vivo rat proximal convoluted tubule. These workers assumed implicitly that all volume flow traversed junctional complexes, and that ionic concentrations in intercellular spaces could be equated with those in the interstitium. Likewise, our previous analysis (31) showed that *equation 22* described dissipative ion transport in these tubules when active ion transport was inhibited.

### *Driving Force for Fluid Absorption*

Our present calculations, as well as our earlier analysis of fluid absorption coupled to passive ion transport (31), apply to a particular set of circumstances, i.e., fluid absorption from proximal straight tubules exposed to asymmetrical solutions. Both in our earlier analysis and in the present model the computed $Na^+$ concentrations (and hence the osmolalities) of lateral intercellular spaces were either the same or slightly less than the external solution osmolalities (Fig. 4); and fluid absorption could be rationalized in terms of the oppositely directed $Cl^-$ and $HCO_3^-$ concentration gradients between lumen and bath, and the fact that junctional complexes were more permeable to $Cl^-$ than $HCO_3^-$.

Some additional insight into the present model may be obtained from the following considerations. Figure 4 indicates that during fluid absorption at 37°C, the computed $Na^+$ concentration in intercellular spaces was very nearly equal to the $Na^+$ concentrations in the perfusate and bath. Likewise, during fluid absorption at 21°C (i.e., fluid absorption coupled to passive ion flows, Table 5), our earlier calculations (31) indicated that the $Na^+$ concentrations in intercellular spaces were practically the same as those shown in Fig. 4. Taking these factors into account, the effective osmotic gradient driving fluid absorption across junctional complexes, either at 21° or at 37°C, may be approximated by expressing *equation 4* as

$$\frac{J_v}{P_f^j \bar{V}_w} \simeq \sigma_{Cl}^j (C_{Cl}^0 - C_{Cl}^1) + \sigma_{HCO_3}^j (C_{HCO_3}^0 - C_{HCO_3}^1) \qquad (23)$$

where $P_f^j$ (Fig. 1), $\sigma_i^j$ (Table 10 for 37°C, and Table 3 for 21°C), and $C_i^0$ (Fig. 4 for 37°C; Fig. 5 in Ref. 31 for 21°C) are functions of $\alpha$. Using the $J_v$ values in Table 5 and the $P_f^j$ values in Fig. 1, the effective osmolality gradients driving fluid absorption are: at 37°C, from 11.6 mosmol liter$^{-1}$, at $\alpha = 1$, to 3.0 mosmol liter$^{-1}$, at $\alpha = 60$; and at 21°C, from 4.6 mosmol liter$^{-1}$, at $\alpha = 1$, to 1.2 mosmol liter$^{-1}$, at $\alpha = 60$. Put another way, the differences between the effective osmolality gradients driving fluid absorption at 37° and at 21°C range from 7 mosmol liter$^{-1}$ at $\alpha = 1$, to 1.8 mosmol liter$^{-1}$, at $\alpha = 60$.

Evaluation of the analytical results in this paper and in our previous paper (31) in terms of *equation 23* indicates that at least two factors contribute to the lower effective osmotic gradient driving fluid absorption at 21° compared to 37°C. First, a comparison of Tables 3 and 10 shows that the computed magnitude of $(\sigma_{HCO_3}^j - \sigma_{Cl}^j)$, for a given value of $\alpha$ was greater at 37° than at 21°C, because $\sigma_{Cl}^j$ was slightly lower at 37° than at 21°C. So it may be that ionic reflection coefficients are slightly different at 37° than at 21°C, although we have no explanation for the physical basis for such changes, if they occur. Second, the anion concentrations at x = 0 may vary at 21° and at 37°C. Figure 4 shows that at 37°C, both the concentrations of $Cl^-$ and $HCO_3^-$ at x = 0 were very slightly less than in the bathing solutions. In contrast, our earlier analysis (31) of fluid absorption coupled to passive ion flows at 21°C yielded computed values of $Cl^-$ and $HCO_3^-$ at x = 0 which were, respectively, higher and lower than in the bathing solutions. Therefore, in terms of *equation 23*, there is a proportionate reduction in the driving force for fluid absorption at 21° compared to 37°C.

Finally, $\sigma_{HCO_3}^j$ values listed in Table 10 were computed by assuming that the active transport sites for $Na^+$ and $HCO_3^-$ were uniformly distributed along lateral intercellular spaces. As indicated above, these $\sigma_{HCO_3}^j$ values accounted for the measured rates of fluid absorption. But when the active transport sites were localized to the first 0.2 mm of channel length, nonreal values for $\sigma_{HCO_3}^j$ were obtained (cf. RESULTS). These results are at least consistent with the recent observations of Kyte (19) who found, by immunohistologic techniques, that ($Na^+$ + $K^+$)-dependent ATPase activity was uniformly distributed along the intercellular spaces of canine cortical proximal convoluted tubules.

### *Comparison with Standing Gradient Model*

The standing-gradient model for fluid absorption proposed by Diamond and Bossert (9) considered the case of fluid transport across epithelia exposed to symmetrical salt solutions, while the present model is restricted to the case of fluid transport across proximal straight tubules exposed to asymmetrical salt solutions. As indicated above, the asymmetry of anion concentrations in the perfusing and bathing solutions, coupled to the fact that junctional complexes of these tubules are more permeable to $Cl^-$ than to $HCO_3^-$, provides a driving force for fluid absorption which was not considered in the standing-gradient model of Diamond and Bossert (9). In addition to this difference, there are some major differences in the choice of transport parameters utilized in the present model and by Diamond and Bossert (9) in the standing-gradient model. A consideration of some of these differences may be useful in understanding why our computations predict isotonicity rather than hypertonicity of intercellular spaces.

First, the effective osmotic gradient driving fluid transport is substantially greater in the standing-gradient model than in the present model. Diamond and Bossert (9) chose solute transport rates of 0.5–1.5 × $10^{-8}$ osmol $s^{-1}$ $cm^{-2}$ of apparent epithelial surface area and an external solution osmolality of 0.3 osmol $liter^{-1}$, yielding $J_v$ values of 1.66–5 × $10^{-5}$ $cm^3$ $s^{-1}$ $cm^{-2}$ of epithelial surface area. The $J_v$ at 37°C in the present experiments (Table 8) was 9.76 × $10^{-6}$ $cm^3$ $s^{-1}$ $cm^{-2}$, which is 1.7–5.1 times less than in the standing-gradient model. The transepithelial $P_f$ values utilized by Diamond and Bossert (9) were in the range 0.55–27.5 × $10^{-4}$ cm $s^{-1}$; the $P_f^j$ values used in the present calculations ranged from 466 × $10^{-4}$ cm $s^{-1}$, for $\alpha = 1$, to 2,437 × $10^{-4}$ cm $s^{-1}$, for $\alpha = 60$ (cf. Fig. 1). Thus, $J_v/P_f\ \bar{V}_w$, the effective osmotic gradient driving fluid absorption, was 167–182 mosmol $liter^{-1}$ in the standing-gradient model and 3.0–11.6 mosmol $liter^{-1}$ in the present model for fluid absorption at 37°C.

From the above data, it is evident that the higher effective osmotic gradient required by the standing-gradient model, with respect to the present model, depends in part on the higher $J_v$ values utilized by the former, but primarily on the fact that Diamond and Bossert (9) chose $P_f$ values which were 17–90 times less than those used in the present model, and, indeed, more than tenfold less than the transepithelial ADH-dependent $P_f$ of approximately 200 × $10^{-4}$ cm $s^{-1}$ (23, 30) observed in electrically tight epithelia such as the cortical collecting tubule. In this regard, it is important to note that both Wright et al. (40), on the basis of experimental observations, and ourselves (30), on the basis of experimental and theoretical analyses, have provided evidence indicating that the $P_f$ estimates cited by Diamond and Bossert (9), which derive from steady-state osmotic flux measurements, may have been erroneously low by a factor of more than 10, because of solute polarization phenomena referable to unstirred layer effects.

Second, the rates of solute transport used in the standing-gradient model are appreciably greater than those used in the present model, a choice which increases the steady-state solute influx into intercellular spaces in the former with respect to the latter, and favors the development of intercellular space hypertonicity. As indicated above, Diamond and Bossert (9) chose solute transport rates of 0.5–1.5 × $10^{-8}$ osmol $s^{-1}$ $cm^{-2}$ of apparent epithelial surface area. Table 8 indicates that at 37°C, $J_{Na}$ was 1.52 × $10^{-9}$ eq $s^{-1}$ $cm^{-2}$, giving a solute transport rate of 3.04 × $10^{-9}$ osmol $s^{-1}$ $cm^{-2}$, i.e., between 1.6 and 10 times less than in the standing-gradient model.

In other words, in the present model, the need and/or development of intercellular space hypertonicity has been obviated because the net solute transport rates are appreciably lower, and the hydraulic conductance substantially greater, than in the standing-gradient model. And because the asymmetrical solutions used in the present model result in a driving force for fluid transport not considered in the standing-gradient model.

*Inadequacies of the Model*

We emphasize the tentative nature of the present model. The standard deviation for our experimental data is in the range of 15%, and it is reasonable to state that micropuncture techniques do not, on an average, yield experimental results having significantly greater accuracy. Therefore, it is not possible by present experimental techniques—either with isolated perfused tubules or with in vivo micropuncture—to determine whether a fluid absorbate is isotonic or, as suggested (26) for the proximal convoluted tubule of *Necturus*, very slightly hypertonic. It is interesting to note in this context that the transepithelial electrical resistance of the *Necturus* proximal convoluted tubule is 70 $\Omega \cdot cm^2$ (3). If this value were used as an upper limit to $\alpha$ in *equation 2*, a significant fraction of the total resistance to transepithelial $Na^+$ diffusion would be referable to intercellular spaces, and for such conditions intercellular space hypertonicity might obtain. But as indicated in connection with Fig. 1, only an upper limit of $\alpha = 65$, computed for the case of fluid transport via an extracellular route (Fig. 1), is consistent simultaneously with electrical resistance measurements, isotopic permeability coefficients, and either predicted or measured hydraulic conductivity coefficients in these tubules. Therefore, the present model, depicting virtual equilibrium between bath and intercellular spaces, provides a reasonable way of accounting for the experimental data.

Nor is it possible to ascertain with certainty whether or not the luminal fluid remains absolutely isotonic to bathing solutions. As indicated above in connection with *equation 23*, the effective osmotic gradient required for fluid absorption of 0.4 nl $min^{-1}$ $mm^{-1}$ in these tubules is in the range of 3.0–11.6 mosmol $liter^{-1}$, depending on the value of $\alpha$ selected. So it may be that small reductions in luminal osmolality undetectable by present means, i.e., from a perfusate osmolality of 300 mosmol $liter^{-1}$ to a luminal osmolality of, for example, 297 mosmol $liter^{-1}$, could also provide a driving force for net fluid transport.

Finally, it is evident that the present model is not adequate to account for the rates of fluid absorption observed when these tubules are exposed to symmetrical solutions. For example, when the perfusate and bath are symmetrical $HCO_3$-KR solutions, $J_v$ at 37°C in these tubules is approximately 0.4 nl $min^{-1}$ $mm^{-1}$ (i.e., not very different from the $J_v$ at 37°C with a Cl-KR* perfusate and an $HCO_3$-KR* bath), but the collected fluid [$Cl^-$] only rises to 127.6 mM, and the mean luminal [$Cl^-$] to approximately 122.1 mM; carbonic anhydrase-mediated $HCO_3^-$ absorption accounts for much, but not all, of the rise in the intraluminal [$Cl^-$] (29). Put another way, during spontaneous fluid absorption from symmetrical $HCO_3$-KR solutions, the driving force for fluid absorption generated by a rising intraluminal [$Cl^-$] is smaller than that produced by using a Cl-KR* perfusate. Therefore, it is evident that additional driving forces, for example, the development of luminal hypotonicity, exist for the case of fluid absorption from tubules perfused and bathed with symmetrical solutions.

We are grateful to Dr. L. W. Welling, Veterans Administration Hospital, Kansas City, Missouri for providing us with the $P_f^0$ value for isolated rabbit proximal straight tubules. We thank our research assistants, S. L. Troutman and B. E. Richey, for able assistance in carrying out these experiments.

This work was supported by Research Grant 75-805 from the American Heart Association, BMS 74-13645 from the National Science Foundation, and 5-R01-AM 14873 from the National Institutes of Health.

During the course of these studies, J. A. Schafer was an Established Investigator of the American Heart Association (71-177).

Received for publication 16 August 1976.

## REFERENCES

1. BARRY, P. H., AND J. M. DIAMOND. Junction potentials, electrode standard potentials, and other problems in interpreting electrical properties of membranes. *J. Membrane Biol.* 3: 93–122, 1970.
2. BENNETT, C. M., B. M. BRENNER, AND R. W. BERLINER. Micropuncture study of nephron function in the Rhesus monkey. *J. Clin. Invest.* 47: 203–216, 1968.
3. BOULPAEP, E., AND J. F. SEELY. Electrophysiology of proximal and distal tubules in the autoperfused dog kidney. *Am. J. Physiol.* 221: 1084–1096, 1971.
4. BURG, M., J. GRANTHAM, M. ABRAMOW, AND J. ORLOFF. Preparation and study of fragments of single rabbit nephrons. *Am. J. Physiol.* 210: 1293–1298, 1966.
5. CALDWELL, P. C. Liquid junction potentials and their effect on potential measurements in biological systems. *Intern. Rev. Cytol.* 24: 354–371, 1968.
6. CLAPP, J. R., J. F. WATSON, AND R. W. BERLINER. Osmolality, bicarbonate concentration, and water reabsorption in proximal tubule of the dog nephron. *Am. J. Physiol.* 205: 273–280, 1963.
7. CURRAN, P. F., AND J. R. MACINTOSH. A model system for biological water transport. *Nature* 193: 347–348, 1962.
8. DENNIS, J. W., P. B. WOODALL, AND C. C. TISHER. Phosphate transport in isolated perfused proximal tubule (Abstract). *Ann. Meeting Am. Soc. Nephrol., 7th, Washington, D.C., 1974,* p. 22.
9. DIAMOND, J. M., AND W. H. BOSSERT. Standing-gradient osmotic flow, a mechanism for coupling of water and solute transport in epithelia. *J. Gen. Physiol.* 50: 2061–2082, 1967.
10. FRÖMTER, E., G. RUMRICH, AND K. J. ULLRICH. Phenomenologic description of $Na^+$, $Cl^-$ and $HCO_3^-$ absorption from proximal tubules of the rat kidney. *Pfluegers Arch.* 343: 189–220, 1973.
11. GOTTSCHALK, C. W. Renal tubular function: lessons from micropuncture. *Harvey Lectures, Ser. B.* 58: 99–124, 1962–63.
12. GOTTSCHALK, C. W., W. E. LASSITER, AND M. MYLLE. Localization of urine acidification in the mammalian kidney. *Am. J. Physiol.* 198: 581–585, 1960.
13. GRANTHAM, J. J., P. B. QUALIZZA, AND L. W. WELLING. Influence of serum proteins on net fluid reabsorption of isolated proximal tubules. *Kidney Intern.* 2: 66–75, 1972.
14. HODGKIN, A. L. The ionic basis of electrical activity in nerve and muscle. *Biol. Rev.* 26: 339–409, 1951.
15. KAWAMURA, S., M. IMAI, D. W. SELDIN, AND J. P. KOKKO. Characteristics of salt and water transport in superficial and juxtamedullary straight segments of proximal tubules. *J. Clin. Invest.* 55: 1269–1277, 1975.
16. KEDEM, O., AND A. KATCHALSKY. A physical interpretation of the phenomenological coefficients of membrane permeability. *J. Gen. Physiol.* 45: 143–179, 1961.
17. KEDEM, O., AND A. LEAF. The relation between salt and ionic transport coefficients. *J. Gen. Physiol.* 49: 655–662, 1966.
18. KOKKO, J. P., M. B. BURG, AND J. ORLOFF. Characteristics of NaCl and water transport in the renal proximal tubule. *J. Clin. Invest.* 50: 69–76, 1971.
19. KYTE, J. Immunoferritin determination of ($Na^+$ and $K^+$) ATPase over the plasma membranes of renal convoluted tubules. II. Proximal segment. *J. Cell Biol.* 68: 304–318, 1976.
20. LUTZ, M. D., J. CARDINAL, AND M. B. BURG. Electrical resistance of renal proximal tubule perfused in vitro. *Am. J. Physiol.* 225: 729–734, 1973.
21. MACINNES, D. A. Galvanic cells with liquid junction potentials. In: *The Principles of Electrochemistry.* New York: Dover, 1961, p. 220–245.
22. MALNIC, G., H. ENOKIBARA, M. M. AIRES, AND F. L. VIEIRA. Die Wirkung von Furosemid und NaCl-Belastung auf die Chloridauscheidung im Einzelnephron der Rattenniere, *Pfluegers Arch.* 309: 21–27, 1969.
23. NEUMANN, K. H., AND F. C. RECTOR. Mechanism of NaCl and water reabsorption in the proximal convoluted tubule of the rat kidney. Role of chloride concentration gradients. *J. Clin. Invest.* 58: 1110–1118, 1976.
24. PATLAK, C. S., D. A. GOLDSTEIN, AND J. F. HOFFMAN. The flow of solute and solvent across a two-membrane system. *J. Theoret. Biol.* 5: 426–442, 1963.
25. RAMSAY, J. A., R. H. J. BROWN, AND P. C. CROGHAN. Electrometric titration of chloride in small volumes. *Exptl. Biol.* 32: 822–829, 1955.
26. SACKIN, H., AND E. L. BOULPAEP. Models for coupling of salt and water transport. *J. Gen. Physiol.* 66: 671–733, 1975.
27. SAUER, F. Nonequilibrium thermodynamics of kidney tubule transport. In: *Handbook of Physiology. Renal Physiology,* edited by J. Orloff and R. W. Berliner. Washington, D.C.: Am. Physiol. Soc., 1973, p. 399–414.
28. SCHAFER, J. A., AND T. E. ANDREOLI. Cellular constraints to diffusion. *J. Clin. Invest.* 51: 1264–1278, 1972.
29. SCHAFER, J. A., AND T. E. ANDREOLI. Anion transport processes in the mammalian superficial proximal straight tubule. *J. Clin. Invest.* 58: 500–513, 1976.
30. SCHAFER, J. A., C. S. PATLAK, AND T. E. ANDREOLI. Osmosis in cortical collecting tubules. *J. Gen. Physiol.* 64: 201–227, 1974.
31. SCHAFER, J. A., C. S. PATLAK, AND T. E. ANDREOLI. A component of fluid absorption linked to passive ion flows in the superficial pars recta. *J. Gen. Physiol.* 67: 445–471, 1975.
32. SCHAFER, J. A., C. S. PATLAK, AND T. E. ANDREOLI. Isotonic intercellular spaces during fluid absorption coupled to active salt transport in the pars recta (Abstract). *Clin. Res.* 24: 411A, 1976.
33. SCHAFER, J. A., S. L. TROUTMAN, AND T. E. ANDREOLI. Volume reabsorption, transepithelial potential differences, and ionic permeability properties in mammalian superficial proximal straight tubules. *J. Gen. Physiol.* 64: 582–607, 1974.
34. SMITH, G. D. *Numerical Solutions of Partial Differential Equations.* London: Oxford, 1965, p. 10.
35. ULLRICH, K. J. Permeability characteristics of the mammalian nephron. In: *Handbook of Physiology. Renal Physiology,* edited by J. Orloff and R. W. Berliner. Washington, D.C.: Am. Physiol. Soc., 1973, p. 377–398.
36. VIEIRA, F. L., AND G. MALNIC. Hydrogen ion excretion by rat renal cortical tubules as studied by an antimony microelectrode. *Am. J. Physiol.* 214: 710–718, 1968.
37. WARNOCK, D. G., AND M. B. BURG. Urinary acidification: $CO_2$ transport by the rabbit proximal straight tubule. *Am. J. Physiol.* 232: F20–F25, 1977.
38. WARREN, Y., R. G. LUKE, M. KASHGARIAN, AND H. LEVITIN. Micropuncture studies of chloride and bicarbonate absorption in the proximal renal tubule of the rat in respiratory acidosis and in chloride depletion. *Clin. Sci.* 38: 375–383, 1970.
39. WELLING, L., AND J. J. GRANTHAM. Physical properties of isolated perfused renal tubules and tubular basement membranes. *J. Clin. Invest.* 51: 1063–1075, 1972.
40. WRIGHT, E. M., A. P. SMULDERS, AND J. McD. TARMEY. The role of the lateral intercellular spaces and solute polarization effects in the passive flow of water across the rabbit gallbladder. *J. Membrane Biol.* 7: 198–219, 1972.